공학석사 학위논문

Development of Injectable Microcryogel System for Delivering Therapeutic Agents

치료제 전달을 위한 주사가능한
마이크로 크라이오겔 시스템 개발

2020년 8월

서울대학교 대학원
협동과정 바이오엔지니어링 과정

박 민 정

Development of Injectable Microcryogel System for Delivering Therapeutic Agents

지도 교수 Nathaniel Suk-Yeon Hwang

이 논문을 공학석사 학위논문으로 제출함

2020년 8월

서울대학교 대학원

협동과정 바이오엔지니어링 과정

박 민 정

박민정의 공학석사 학위논문을 인준함

2020년 8월

위 원 장 백 승 렬 (인)

부위원장 Nathaniel Suk-Yeon Hwang (인)

위 원 김 병 수 (인)

ABSTRACT

Development of Injectable Microcryogel System for Delivering Therapeutic Agents

Mihn Jeong Park
Interdisciplinary Program in Bioengineering
The Graduate School of Engineering
Seoul National University

Cryogels have a large porous structure, and they can be tailored to have shape-memory ability and injectability. In addition, cells or growth factors can be loaded within the cryogel and show sustained release behavior. Because of these characteristics, the cryogels have been widely used for tissue-engineering applications.

However, bulky cryogel cannot pass the narrow needle syringe and fill the irregular shape defect perfectly. Herein, we established an injectable cryogel system for delivering cells or therapeutic agents. It displayed smoothly injectable characteristics that exhibited printability and void-filling ability.

In chapter one, we fabricated injectable cryogel microparticles (CMP) *via* simply pulverizing. To prepare the CMP, we used both methacrylated chitosan (Chi-MA) and methacrylated chondroitin sulfate (CS-MA) and cross-linked them under -20℃ conditions. Also, we loaded the recombinant human-vascular endothelial growth factor (rhVEGF) into the CMP (V-CMP), and the sustained release behavior could be obtained. Finally, when the V-CMP were injected into mice hindlimb ischemia model, the enhanced neovascularization and effective tissue necrosis prevention were observed.

In chapter two, we also fabricated injectable cryogel microsphere *via* microfluidic and emulsification. The microspheres consist of methacrylated gelatin (Gel-MA) and methacrylated hyaluronic acid (HA-MA), and they had narrow size distribution. In addition, we confirmed that the cells could infiltrate into the cryogel microspheres and that the microspheres provided the cells with favorable environment.

Key words; injectable cryogel, sustained release, microparticle, microsphere, neovascularization, cell delivery
Student number; 2018-28698

Table of Contents

List of figures

CHAPTER ONE:

Enhanced Neovascularization Using Injectable and rhVEGF-Releasing Microparticles

1. Introduction

Cryogels have an interconnected macroporous structure formed by the ice crystal-mediated pore formation at low temperatures [1, 2]. Due to their spongy-like structure, the cryogels can imbibe a large amount of water and still retain shape-memory and deformability. These unique characteristics of cryogels have enabled them to be applied as injectable scaffolds system [3]. The injectable cryogels have been utilized to treat dilaceration or the occasions needed for open surgery in a minimally invasive way [4, 5]. However, it is often suffered from injecting cryogels through the narrow needle. Furthermore, since the cryogels would remain in their original shape after injection, it is not appropriate to inject them into irregular wounds or dense tissues

such as muscle tissue [6, 7]

The cryogels have also been used as a delivery carrier of cells, drugs, and macromolecules to improve the therapeutic outcomes [8–10]. Among various methods for delivering the growth factors, the strategy based on the electrostatic attraction with the cryogels has been extensively studied [11]. For examples, glycosaminoglycans (GAGs) have carboxyl and sulfate groups that display negative charge, e.g., heparin, heparan sulfate, chondroitin sulfate (CS), which have an excellent binding affinity with various growth factors such as vascular endothelial growth factor (VEGF), basic fibroblast growth factor (bFGF), and platelet-derived growth factor (PDGF) [12, 13]. Heparan sulfate has been incorporated into cryogels for sustained release of growth factors by having a charge-dependent affinity [14]. Likewise, CS is also negatively charged, allowing for potential electrostatic interaction with cationic drugs and protein molecules [15]. They have also been used in the combinatorial system with other polycationic biopolymers, including chitosan (Chi), to control the release kinetics of growth factors [16-18]. These biopolymers are often engineered to finely control the release kinetics of growth factors [19, 20].

In this study, we developed an injectable cryogel

microparticle (CMP) by simply pulverizing the bulky cryogels aim at improving the injectability (Scheme 1). We fabricated a cryogel by cross-linking CS-methacrylate (CS-MA) and Chi-methacrylate (Chi-MA). The gel-like properties were obtained by dispersing the CMP in an aqueous phase, and its mechanical and injectable properties were characterized. Furthermore, we loaded rhVEGF into the CMP (V-CMP) with anticipating the CS-mediated sustained release of the rhVEGF. Finally, the therapeutic efficacy of the V-CMP was estimated *via* intramuscular injection into mice hindlimb ischemia model. It highlights that we could improve the injectability of the cryogel, and this study would broaden its applicability to tissue engineering and regeneration medicine.

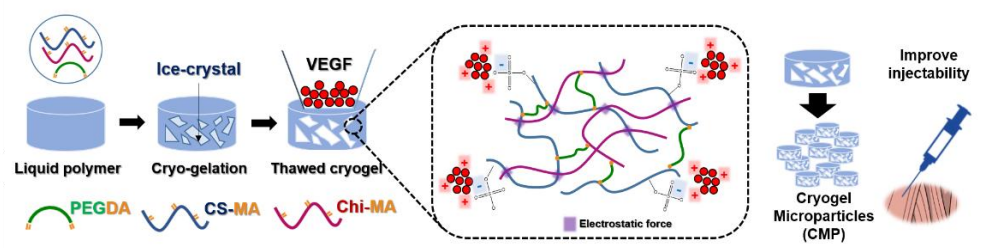

Scheme 1 The schematic of fabricating the cryogel microparticle (CMP). The cryogel was prepared by cross-linking of Chi-MA/CS-MA/PEGDA at -20℃. The rhVEGF could be entrapped into the cryogel due to the electrostatic force with negative charges of CS-MA, displaying the sustained release kinetics of the rhVEGF. The bulky cyrogel was pulverized into the micron-sized particles and dispersed within an aqueous phase, which enabled the CMP to be injectable through the narrow syringe needles.

2. Experimental section

2.1 Synthesis of methacrylated biopolymers

Chitosan methacrylate (Chi-MA) was synthesized, as previously reported [21]. Briefly, Chitosan (MW: 50,000-190,000 Da, 448869, Sigma-Aldrich) was dissolved in 2 % acetic acid solution at 1.0 w/v % until the clear solution was obtained at room temperature. Methacrylic anhydride (276685, Sigma-Aldrich) was added at a 0.4 molar ratio to the chitosan unit. After reacting for 3 hours at RT, the solution was dialyzed (3.5K MWCO) against distilled water for two days to eliminate the unreacted reagents, followed by lyophilization and storage at −20℃. The methacrylation was confirmed by ^{1}H NMR by dissolving both chitosan and Chi-MA in 0.25% DCl-containing D_2O (0.5 w/v%).

Chondroitin sulfate-methacrylate (CS-MA) was also synthesized as previous work [22]. Chondroitin sulfate (C0335, Tokyo Chemical Industry Co., Ltd.) was dissolved in phosphate-buffered saline (PBS) at 10 w/v %. It was reacted with glycidyl methacrylate (151238, Sigma-Aldrich) (73mM) for 11days to conjugate methacrylate functional groups. Then, the reaction was stopped by dialysis through a membrane (3.5K MWCO) for 48 hours, followed by lyophilization and storage at −20℃ for further use. The

methacrylation of C.S. was also confirmed by ^{1}H NMR by dissolving the polymers in D_2O.

2.2 Fabrication of cryogels

For fabricating the cryogels, poly(ethylene glycol) diacrylate (PEGDA) (MW: 3,400 Da, 46497, Alfa Aesar) was used as cross-linker. The final concentration of Chi-MA and PEGDA were 0.5 and 2.5 w/v %, and that of CS-MA was varying from 0.5 to 2.5 w/v %. Ammonium persulfate (APS) (A3687, Sigma-Aldrich) and N,N,N′-tetramethylethylenediamine (TEMED) (Sigma-Aldrich) were added to the solution at 0.4 w/v % and 0.1 v/v %, respectively. Then the polymerization was proceeded for 18 hours at -20℃, followed by lyophilization.

2.3 Characterization of cryogels

The swelling ratio was characterized by measuring both the dry and wet weight of the cryogel. The wet weight was measured after soaking the cryogel in DI water until it reached the swollen equilibrium state. The swelling ratio was calculated as the following equation;

$$\text{Swelling ratio } (Q) = W_s/W_d$$

, where W_s and W_d represent swollen and dry weight, respectively.

The mechanical property of the cryogel was estimated using a rheometer (MCR 302, Anton-Paar, Austria) depends on the amount of CS-MA. The cryogels were prepared in a cylindrical shape with a diameter of 8 mm. The frequency sweep test was carried out with increasing the oscillator frequency from 0.1 to 10^2 Hz at a constant strain of 1 %. The shear storage modulus (G') and loss modulus (G") were recorded.

To investigate the compositional homogeneity of cryogel, FITC-labeled Chi-MA and RITC-labeled CS-MA were prepared as previously reported [23, 24]. After fabricating the cryogel, the fluorescent images were obtained through a fluorescent microscope (EVOS, AMF4300, EVOS, Life Technology).

2.4 Fabrication of cryogel microparticle (CMP)

To obtain the CMP, the bulk cryogel with a CS-MA concentration of 2.5 w/v % was ground using a pulverizing machine (RT-02A, Rong Tsong Precision Tech. Co., Taiwan) in a dried state. The particular shape was observed in both dried and swollen state through an optical microscope, and their size distributions were determined from the images using Image J (Image J Software).

2.5 Rheological properties and injectability of the CMP

The rheological properties and injectability of the CMP were investigated with soaking in PBS with different particle concentrations. The CMP was dispersed at 5 and 10 w/v % (CMP-5 and CMP-10, respectively). Each CMP dispersion was loaded between the measurement cells of the rheometer, whose gap was 1.5 mm (Measuring cell: P-PTD & H-PTD 200). Viscosity measurement, strain sweep test, and continuous step strain test were carried out. Firstly, the viscosity was measured varying the shear rate from 1 to 10^3 1/s. Secondly, in the strain sweep test, both the shear storage and loss modulus (G' and G") were recorded at a strain range from 0.1 to 500 % with a frequency of 10 Hz. Finally, the shape recovery ability of the CMP dispersion was analyzed from the cyclic strain test by alternating 1 % and 500 % strain minutely for 5 min. In addition, the injectability was confirmed by extruding the CMP-10 through a 23G needle into either the PBS bath or pre-shaped molds.

2.6 Release kinetic analysis

The release behavior of the recombinant human-vascular endothelial growth factor (rhVEGF) was analyzed. The rhVEGF was added to the CMP-10 at 10 ng/mL and stored at 4℃ overnight. The 100 μL of rhVEGF-loaded CMP-10 (V-CMP) was placed on the upper chamber of transwell, while the lower chamber was filled with PBS. During incubation at 37℃ in a humidified atmosphere, the release behavior was investigated. Using enzyme-linked immunosorbent assay (ELISA), the release amount of rhVEGF was determined, and its cumulative amount was calculated.

2.7 Antibacterial test

The antibacterial ability of the Chi-MA/CS-MA/PEGDA cryogel was tested with *Escherichia.coli (E.coli)* and *Staphylococcus aureus (S.aureus)* by absorbance estimation (OD 600nm). Bacterial cells were inoculated on agar plate for growth. After incubating the bacterial cells, the cryogel was soaked in bacterial media. Measure the absorbance at 600nm.

2.8 *In vitro* biocompatibility and cell proliferation

The effects of rhVEGF released from the CMP on cellular behavior were estimated. Human umbilical vein endothelial cells (HUVECs) were seeded on the lower chamber, and the V-CMP was placed on the upper chamber of the transwell. The same amount of rhVEGF (10 ng/mL) was added into the culture medium as a positive control, and the CMP (without rhVEGF) was also tested. The cells were maintained with EGM^{TM}-2 signleQuots® (CC-3162, Lonza, Walkersville, MD) without the rhVEGF component. After five days, the cell viability was confirmed using the Live/Dead assay kit (Invitrogen), and the fluorescent images were obtained using a fluorescence microscope (AMF4300, EVOS, Life Technology). The cell viability was calculated from the number of live cells per total cells.

The *in vitro* cell proliferation was monitored as the way of cell viability test. The metabolic activity of the cells was confirmed by Presto blue cell viability reagent (A13261, Invitrogen) following the manufacturer's protocol. The fluorescence intensity of the reacted solution was measured at λ_{ex} = 560 nm and λ_{ex} = 590 nm, followed by calculating the relative cell proliferation.

2.9 *In vivo* hindlimb ischemia model and cryogel injection

All the *in vivo* experimental procedures were approved by IACUC of Seoul National University (SNU-190917-5). Eight weeks female balb/c mice (OrientBio Co., Republic of Korea) were used, and the surgery was carried out under isoflurane anesthesia. After the hair was removed, the left lower extremity is disinfected with betadine solution. The skin was incised in 2 to 3 cm, along the left femoral artery. The blood flow was blocked by ligation with a 3-0 silk suture from the lower part of the inferior epigastric artery to the midpoint of the superficial femoral artery [25, 26]. After the surgery, the ischemic hindlimbs of mice were treated by injecting 100 μL of PBS, CMP-10, rhVEGF, and rhVEGF-CMP-10 into the musculus gracilis. The extent of necrosis of the hindlimb ischemia area was analyzed until 28 days. The blood flow of each limb was measured *via* a laser Doppler perfusion imaging (LDPI) weekly, and its perfusion was quantified using colored histogram pixel expressed as LDPI index, which means the ratio of the ischemic limb to the normal limb bloodstream. The tissue salvage score was measured as previously reported [14, 27]. Briefly, the hindlimb tissues were scored by a semiquantitative scale: entire recovery (score 6), minor necrosis or nail loss (score 5), partial toe amputation (score 4),

total toe amputation (score 3), partial/total foot amputation (score 2), or partial/total limb amputation (score 1).

2.10 Histological analysis

After four weeks of treatment, the inguinal muscle tissues were collected and fixed with formaldehyde (4 w/v%). The tissues were paraffin-embedded and sectioned into 10 μm, followed by hematoxylin and eosin (H&E) staining. In addition, for investigating the angiogenic response, the tissue sections were processed to perform the immunofluorescence staining. The specimens were incubated with a primary antibody α-SMA (Anti-alpha smooth muscle Actin antibody, ab5694, Abcam), followed by visualization using the goat anti-rabbit secondary antibody (Alexa Fluor® 594, ab150080, Abcam) and 4′,6-Diamidine-2′-phenylindole dihydrochloride (DAPI) staining.

2.11 Statistical analysis

All data are presented as the mean ± standard deviation. Statistical significance between groups was determined by Student's t-test with $*p< 0.05$, $**p< 0.01$, and $***p< 0.005$.

3. Results & Discussion

3.1 Synthesis of methacrylated biopolymers

We synthesized both Chi-MA and CS-MA by methacrylation process and conducted the ^{1}H-NMR analysis. The ^{1}H-NMR spectra of Chi-MA represented the peaks from 1.8 to 2.3 ppm corresponding to protons in the methacrylamide and the acetyl moieties, and the peaks of methylene and methacrylamide from 5.2 to 6 ppm also appeared (Figure 1A) [28]. At the same time, the ^{1}H-NMR spectra of CS-MA showed the peaks at 1.89, 5.7, and 6.11 ppm corresponding to the methacrylate group (Figure 1B), which indicated that both the Chi-MA and CS-MA were successfully synthesized.

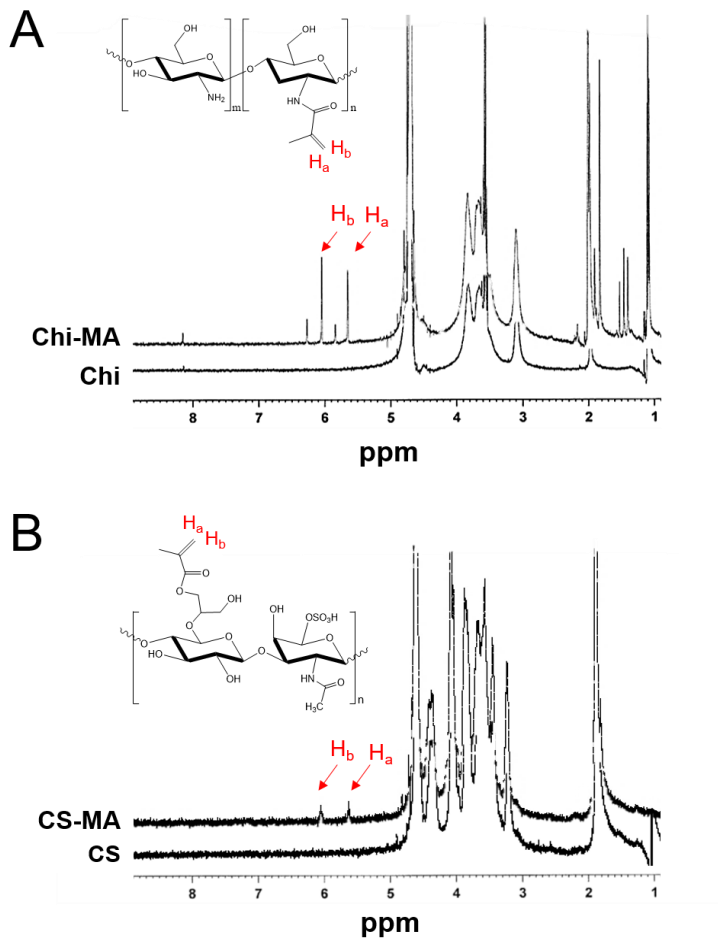

Figure 1 ^{1}H-NMR analysis of the methacrylated biopolymers. ^{1}H-NMR spectra of (A) chitosan methacrylate (Chi-MA) and (B) chondroitin sulfate methacrylate (CS-MA). The peaks corresponding to the methacrylate group were confirmed, which indicated that both Chi-MA and CS-MA were successfully synthesized.

3.2 Fabrication and characterization of the Chi-MA/CS-MA/PEGDA cryogels

The cryogels are formed at subzero temperatures, and their properties could be controlled dependent on cryogelation time, polymeric molecular weight, and initiator concentration [29]. Through the process, cryogels have interconnected macroporous structure, which contributes to offering injectability with immediate shape recovery [30].

The physical and mechanical characteristics of GAGs-based cryogel scaffolds can be tunable depending on their charge freezing time, polymer molecular weight or cooling rate, etc. [31]. Here, Chi-MA was used to strengthen the cryogel mechanical property by electrostatic interaction with CS-MA, as previously reported [32] . Also, we characterized the cryogels by tuning the amount of CS-MA (0, 0.5, 1, and 2.5 w/v %), since the sulfate groups of CS allowed the cryogels to significantly uptake the water. Poly(ethylene glycol) diacrylate (PEGDA) was used as a cross-linker, and it could retain the structural stability of the cryogels (Figure S1). The cryogels could imbibe the water and be immediately swollen regardless of CS-MA contents (Supplementary Video 1); however, the volumetric swelling ratio of the cryogels increased with increasing the CS-MA

contents due to the abundant hydrophilic and negative charge moieties of CS (Figure 2A). The Q value of 2.5% CS-MA cyrogel represented 24.82 ± 1.6 while those of 0, 0,5, and 1.0% CS-MA cryogels were 18.38 ± 2.35, 18.3 ± 2.31, and 20.11 ± 2.52 respectively (Figure 2B). It suggests that the hydrophilic moiety of CS-MA was contributed to holding a much more aqueous solution, which would result in a high loading efficiency of growth factors. Next, we analyzed the mechanical property of the cryogel dependent on CS-MA contents. The CS-MA-deficient cryogels exhibited the highest shear modulus (Figure 2C). However, in the case of CS-MA-containing cryogels, there was a tendency of having incremented shear modulus along with the higher CS-MA-contents. It might be attributed to the increase of polymers contents in the cryogels.

The various biomimetic scaffolds, consist of both Chi and CS, have been fabricated via forming polyelectrolyte complex; however, the electrostatic interaction may often lead to randomly aggregated- and non-homogeneous scaffolds [33-35]. Thus we estimated whether the mixture of Chi-MA and CS-MA could fabricate the homogeneous cryogel scaffolds. After conjugating the distinct fluorescent dyes to both Chi-MA and CS-MA, respectively, then we inspected the

distribution of each polymer within the cryogel through a fluorescent microscope (Figure 2D). We could observe that FITC-labeled Chi-MA (green) and RITC-labeled CS-MA (red) were homogeneously distributed within the cryogel. As a result, we confirmed that the physical and mechanical properties of the cryogels could be adjusted by varying the amount of CS-MA. Subsequently, we proceeded with using 2.5 w/v% CS-MA in the following experiments.

A cationic polysaccharide, Chi have been widely used to fabricate polyelectrolyte complex with anionic biomaterials, such as CS and heparan sulfate, through ionic coacervation [17, 18]. We successfully cross-linked the CS-MA and Chi-MA using PEGDA as a cross-linker, and the homogenous cryogel scaffold was obtained without phase separation (Figure 2).

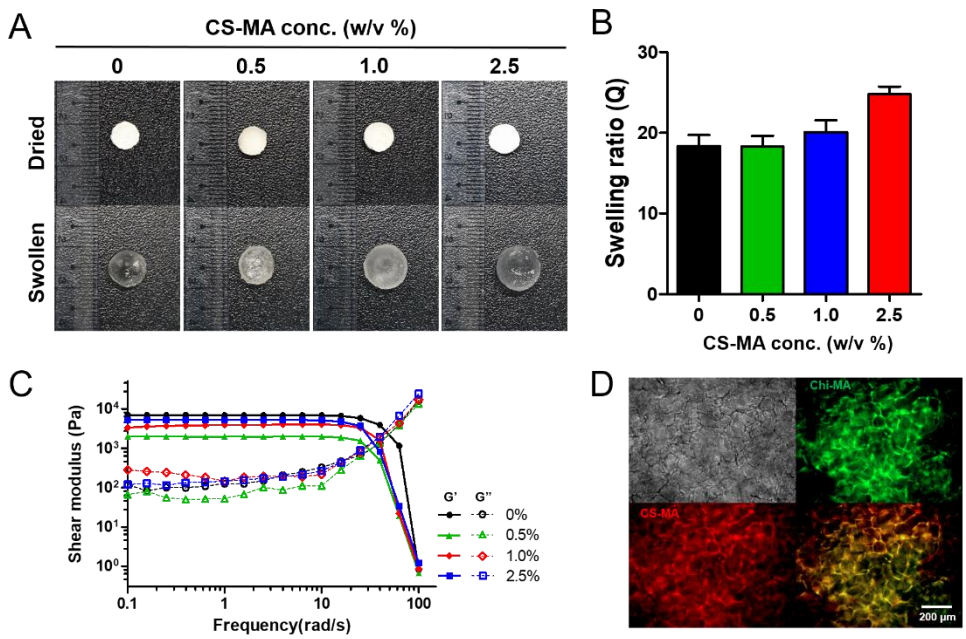

Figure 2 Fabrication and characterization of Chi-MA/CS-MA/PEGDA cryogel. (A) The photographs of the cryogels in both dried and swollen states, which showed the higher volumetric swelling was obtained with increasing the CS-MA content. (B) The swelling ratio (Q) of the cryogels depending on the amount of CS-MA. (C) The shear storage modulus (G') and loss modulus(G") of the cryogels were measured by the frequency sweep test. (D) The fluorescent images of cryogels consist of FITC-labeled Chi-MA and RITC-labeled CS-MA, which revealed that Chi-MA and CS-MA were homogenously mingled throughout the cryogel.

3.3 Preparation of the cryogel microparticle (CMP) and the injectability

The injectable biomaterials are beneficial to be used for filling the wounds or damaged tissues with irregular shape and used as delivery carriers of therapeutic agents [36, 37]. The injectable system can also facilitate the surgical procedure, such as intramuscular injection and intrasynovial injection [38, 39]

Here, we ground the bulky cryogel to improve the injectability through a pulverizing machine and observed the microscopic images in both dried and swollen states in PBS (Figure 3A). The CMP contained micron-sized grains with irregular structures, and each particle increased in size when swollen like bulky cryogel. Particularly, the swollen CMP showed an areal particle size distribution of about from 1.0×10^4 to 10×10^4 μm^2, whereas displaying about from 0.5×10^4 to 5.0×10^4 μm^2 in the dried state (Figure 3B). The most substantial portion was ranging in size from 1.5×10^4 to 5.5×10^4 in the swollen state and from 0.5×10^4 to 2.5×10^4 μm^2 in the dried state.

In the case of injectable biomaterials and viscosupplementation (e.g., dermal fillers), the injectable properties can be affected by both the molecular weight and cross-linking

degrees of the ingredients [40]. Likewise, by mixing it with an aqueous phase in different concentrations, we investigated the effect of CMP content on its rheological properties. The amount of CMP in PBS was set as 5 (CMP-5) and 10 w/v % (CMP-10). CMP-10 and CMP-5 had a viscosity of about 129 and 27.0 Pa-s, respectively (Figure 3C). In both CMP, as the shear rate increased, the viscosity decreased, implying that the CMP system has shear-thinning property and can pass the syringe needle. We also estimated the shear moduli (G' and G") of both CMP under the strain sweep condition. In the absence of strain, CMP-10 showed G' of 1.15 kPa, and CMP-5 of 0.16 kPa (Figure 3D). Both CMP showed that their G' was higher than G", which suggests that both CMP had gel states. However, as the shear strain was increased, the gel-sol transition (G' <G") occurred in CMP-10 and CMP-5 at about 194 and 121 %, respectively. Based on the breakage strain of the CMP, the oscillatory shear strain (1 % and 500 %) was applied alternately to determine whether the CMP system had self-healing ability (Figure 3E). Both CMP showed a reversible sol-gel transition and exhibited a stable self-healing behavior, demonstrating that the CMP would recover its gel state after passing the needles as a sol-like state. Finally, we confirmed the practical injectability using CMP-10 (Figure 3F(i)). It

was shown that the CMP particles were smoothly injectable through a 23G needle. Furthermore, CMP-10 could retain its structure even injected into the mold with irregular shapes (Figure 3F(ii) and (iii)).

As a result, we found that our CMP system displayed excellent injectability with self-healing behavior, which suggests that it would be readily applied to the diseased or damaged tissues with irregular shapes. It should be noted that this pulverization method is not limited to the Chi-MA/CS-MA/PEGDA cryogel, and can be utilized regardless of the cryogel materials. In fact, we investigated whether other cryogel systems could also be processed with pulverization using gelatin/heparin cryogel [14], and the similar rheological and injectable properties was achieved (data were not shown). This implies that the pulverization-based strategy can broaden the applicability of cryogels.

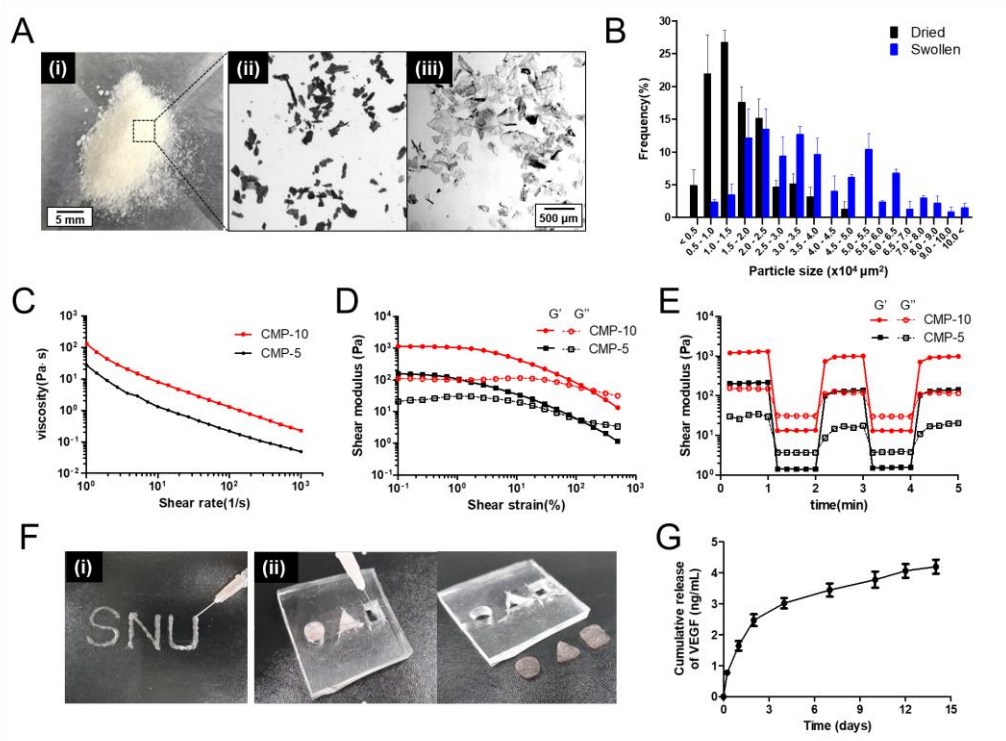

Figure 3 Preparation of the cryogel microparticles (CMP) and its rheological and injectable properties. (A) (i) Photograph of pulverized cryogel. The microscopic image of CMP in (ii) dried and (iii) swollen state. (B) The particle size distribution of CMP was determined based on the microscopic images. (C) Viscosity of both CMP showed the shear-thinning property. (D) The shear moduli were measured by the strain sweep test, which showed that CMP-10 had higher shear modulus and resistance to shear force-mediated breakage than CMP-5. (E) The self-healing ability of both CMP was confirmed by the dynamic strain sweep test with alternately applying oscillatory shear strain (1 % and 500 %). (F) Visualization of the injectability of CMP-10 by injecting it in (i) ambient condition and (ii) the void-filling ability of the CMP-10. (G) Sustained release of rhVEGF from CMP-10 for 15 days

3.4 Sustained rhVEGF-release behavior

A variety of angiogenic agents, such as engineered cells, peptides, and growth factors, have been widely applied to treat cardiovascular diseases [25, 41, 42]. However, the injection of these therapeutic agents alone is not recommended due to the reasons, such as the low survival rate of cells, unstable features of peptides, and the declined targeting efficiency [43]. It has been demonstrated that VEGF plays a pivotal role in neovascularization by inducing proliferation and tube formation of endothelial cells [44]. For enhancing the delivery efficacy of VEGF, polysaccharide biomaterials have been used as a reservoir to incorporate the VEGF [45]. Since the covalent conjugation of VEGF often suffers from the loss of its biological activity, another strategy has emerged using the electrostatic interaction between VEGF and the biomaterials having negatively charged moieties [46]. CS is one of the proteoglycans possessing a negative charge from sulfated groups and have been used for controlled growth factor delivery [47].

Electrostatic interactions of GFs with biomaterials can prolong their release duration, which can lead to promising outcomes for treating diseased or damaged tissues [18, 48]. We anticipated the chondroitin sulfate would entrap the rhVEGF *via* electrostatic

interaction. We evaluated the released kinetics of rhVEGF from CMP-10 with a concentration of 10 ng/mL. The initial burst release was observed within three days, and then the release rate was declined. This sustained-release lasted up to 14 days, showing that the CS-mediated binding of rhVEGF to CMP-10 resulted in the prolonged-release behavior (Fig. 3G). Albeit we thought that the VEGF was incorporated throughout the surface of the CMP, their binding appearance should be further investigated.

Although we did not validate the controlled release behaviors depending on the amount of CS in the cryogels, the V-CMP showed the sustained release of rhVEGF (Figure 4). It can be considered that increasing the Chi ratio dominantly in this CMP system would be applied to carry the other positively charged therapeutic agents, such as plasmid DNA, hormones, and drugs [49-51].

3.5 Antibacterial test

Chitosan was known to have an antibacterial effect [52]. To verify the microbial efficacy of the cryogel, gram positive (S.aureus) and negative (E.coli) were used. The Control group showed burst growth of bacteria, while the CMP group exhibited a poor growth rate. As the amount of bacteria increases, the absorbance increases.

Therefore, we confirmed the cryogel has ability to prevent bacteria growth.

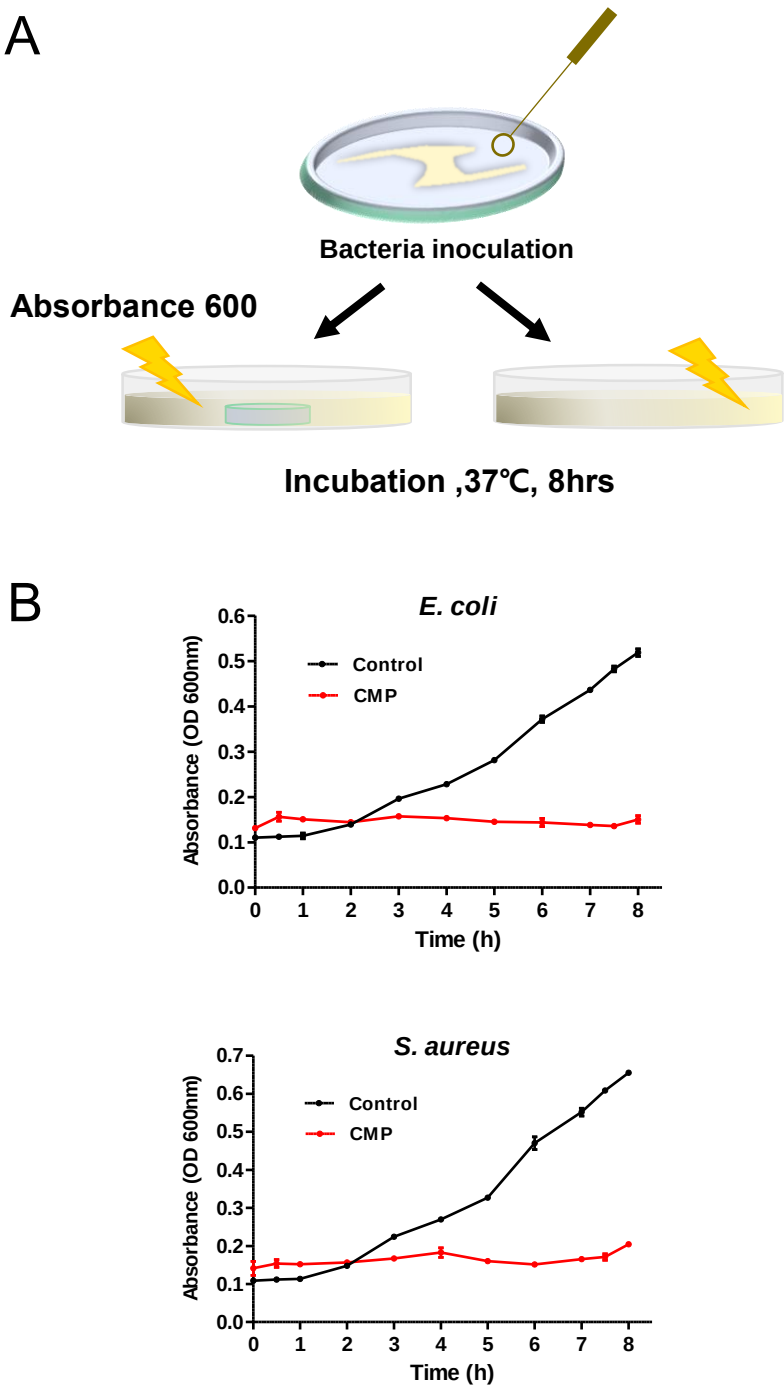

Figure 4 Antibacterial test. (A) Schematic illustration of microbial test. (B) Absorbance at 600nm for E.coli and S.aureus to quantify the amount of bacterial cells.

3.5 The effects of released rhVEGF on cell behavior

We estimated how the rhVEGF released from the CMP-10 could affect the *in vitro* cellular behaviors using human umbilical vein endothelial cells (HUVECs). The bolus rhVEGF was treated as a positive control, and the CMP with and without rhVEGF were placed in the transwell (Figure 5A). Through the Live/Dead analysis, we confirmed that all of the groups had little cytotoxicity, in particular, the cells treated with rhVEGF seemed to spread out much more than cells without rhVEGF treatment (Figure 5B). By quantifying the cell viability based on the Live/Dead images, we confirmed that the rhVEGF-releasing CMP system showed a survival rate of over 95% and did not provide any negative effects on the cells (Figure 5C). Furthermore, through the Prestoblue assay, the effect of release rhVEGF on cell proliferation was assessed (Figure 5D). Although the cells with rhVEGF-CMP displayed a lower proliferation rate than those with bolus rhVEGF, it exhibited a prominently increased proliferation compared to the cells without rhVEGF treatment. It suggests that rhVEGF released from the CMP-10 was effective in cell metabolisms and proliferation.

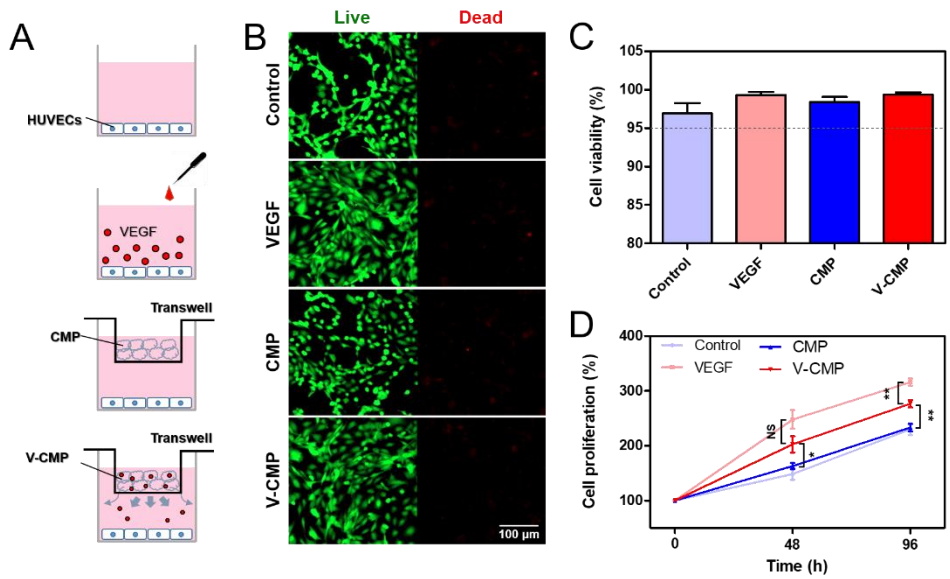

Figure 5 *In vitro* cell proliferation and viability test. (A) Schematic of the in vitro cell test. (B) The fluorescent images of the Live/Dead assay. (C) The quantification of cell viability based on the fluorescent images. (D) The cell proliferation behavior treated with each group, which revealed that the released VEGF from the CMP was effective in cell metabolism.

3.6. Intramuscular injection of the CMP for treating the mice hindlimb ischemia *in vivo*

We assessed the therapeutic efficacy of the rhVEGF-releasing CMP via intramuscular injection into the *in vivo* mice hindlimb ischemia model. The hindlimb ischemia was induced through excising the left femoral artery and treated the mice with the following experimental groups: PBS, VEGF, CMP, V-CMP. Above all, we could assure that the blood flow was successfully blocked through the doppler images. After the injection of each sample, we assessed tissue regeneration and blood perfusion for 28 days (Figure 6A). The PBS (control) group showed paw amputation, while at the same time, the CMP group showed toe amputation. In the case of the VEGF group, the limb tissue almost remained with a little portion of the toe decayed. However, the V-CMP group showed excellent tissue regeneration comparable to the healthy tissue, which might be contributed to the fasted restoration of blood flow (from about two weeks). As a result of quantifying the blood perfusion at four weeks post-treatment, we confirmed that the blood perfusion was recovered slightly by the CMP alone, showing LDPI as 43.2 ± 15.44. The V-CMP had significant resilience by exhibiting the highest LDPI of 90.75 ± 7.33, while VEGF showed LDPI of 70.84 ± 8.13 (Figure

6B). Furthermore, in the tissue salvage score, the VEGF and the V-CMP showed about 4.34 and 5.34, respectively; however, the CMP was inferior to them with showing about 2.67 (Figure 6C). Besides, we conducted histological analysis on the hindlimb tissues at four weeks (Figure 7). The H&E images showed that lots of tissue necrosis occurred in PBS and CMP group, while both the V-CMP and the VEGF exhibited healthy tissue conditions. The V-CMP showed a higher number of α-SMA-positive cells than that of the VEGF, and the newly formed blood vessels in the V-CMP appeared much matured and enlarged. Consequently, we clarified that the CMP could be used in the intramuscular injection and recover the bloodstream by sustained releasing the rhVEGF, which effectively prevented tissue necrosis. Although it should be furhter investigated, the tissue necrosis was slightly prevented than control group and it might be attributed that the CS attracted the surrounding biomolecules, e.g., cytokines, and circulating progenitor cells [53]. In general, microparticle-based injectable systems displayed therapeutic effects with spreading throughout the surrounding tissues [54]. Likewise, it was thought that our CMP-based system effectively delivers the VEGF with steadily dispersed in the muscle tissues. It should be further verified how the biodegradability of

CMP effects on both the release kinetics of VEGF in the *in vivo* environment and tissue regenerative ability. Furthermore, Hou et al. demonstrated that assembly of the microparticles resulted in retention within the target tissues after the *in vivo* injection [55]. This strategy can be utilized to enhance retention of the CMP in tissues using a variety of injectable biomaterials, such as Pluronic-F127 and high-molecular hyaluronic acid. As shown in Figure 3, the CMP dispersed immediately within the aqueous bath, whereas it exhibited sufficient structural stability to be laminated at ambient conditions; therefore, it may be necessary to further study the behavior of the CMP when injected into various biological tissues.

Intramuscular injection of the bulky cryogels may be constrained by the fact that the muscle tissues have highly compact microstructures [56]. Thomas et al. previously fabricated ECM powder by pulverization using a grinding mill and demonstrated the powder would be utilized in tissue engineering applications [57], and several types of research have been conducted using the ground particles [58]. Beyond the above methods, we herein simply developed a pulverized-mediated strategy for fabricating the injectable cryogel system and tried to verify its feasibility of therapeutic application *via* intramuscular injection.

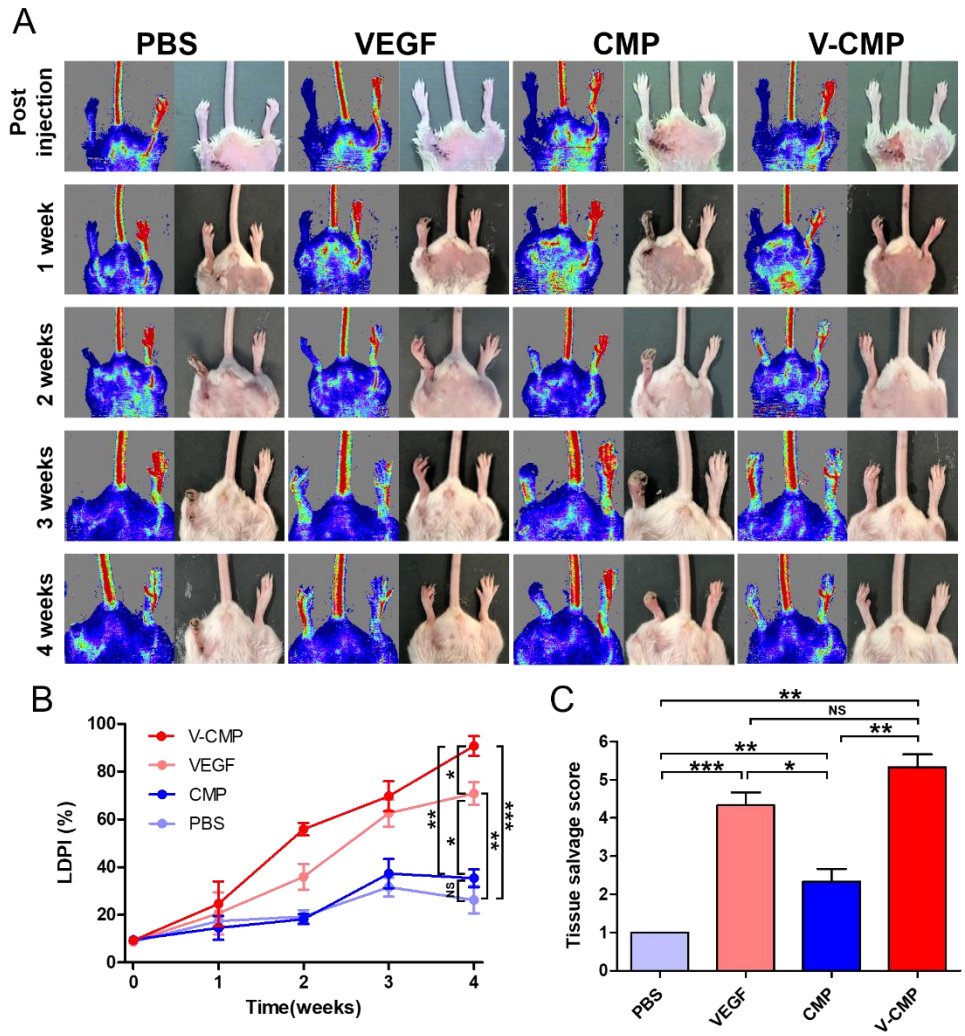

Figure 6 The *in vivo* therapeutic efficacy of V-CMP in mice hindlimb ischemia model. (A) Representative doppler images of hindlimb ischemia mouse injected with PBS (control), VEGF, CMP, and V-CMP during the treatment. (B) Quantitative evaluation of blood perfusion by using Laser Doppler Perfusion Imaging (LDPI). LDPI ratio was determined by comparing the blood flow of the lower limb ischemia to that of healthy tissue. (C) The tissue salvage score of the lower hindlimb regions at four weeks.

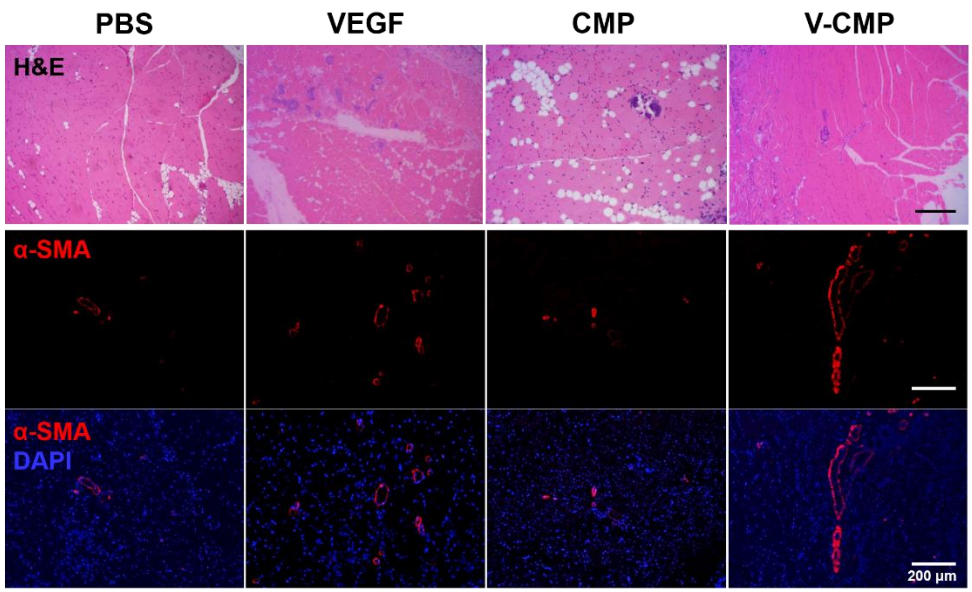

Figure 7 Histological and immunostaining analysis of the ischemia tissues. Histological H&E staining of ischemic muscle tissue was carried out after four weeks. The V-CMP exhibited a highly compact and elaborate tissue structure. Immunostaining images represented that the V-CMP promoted neovascularization in ischemic muscle tissue with showing most abundant α-SMA positive cells (red).

4. Conclusion

In this study, we have proposed an injectable cryogel system using the facile pulverization method. Through the pulverization process, we overcome the size limitation of the injection of bulky cryogels. We fabricated Chi-MA/CS-MA/PEGDA cryogel with optimal ratio, and the physical and mechanical properties were characterized. We confirmed that the CP exhibited the injectability and could readily fill the void area. Furthermore, the VEGF was incorporated into the CP and released in a sustained manner *via* electrostatic interaction with CS-MA. Finally, we proved that this CP-VEGF system promoted neovascularization in the *in vivo* hindlimb ischemia model with preventing tissue necrosis. Consequently, we demonstrated that the pulverization-mediated strategy had the potential to be used for tissue engineering applications.

CHAPTER TWO:

Injectable Cryogel Microsphere for Cell Delivery.

2.1 Introduction

Cell-based therapy has been widely utilized as a strategy for disease treatment and tissue regeneration. Biological scaffolds not only facilitate the delivery of cells to desirable location, but also provide favorable environment to control their migration, proliferation, and differentiation *in vivo*. However, large open surgery is inevitably required to transplant the cell-loaded scaffolds, which poses a potential risk during the operation [59]. Recently, injectable biomaterials have been developed for a minimally invasive therapy and used in various medical treatments. It can reduce patients' pain and provide safety [60].

Hydrogel-based injectable biomaterials have been used as fillers based on the shear-thinning property, but the biological functions of the cells inside the hydrogel were mostly affected due to the low diffusion rate (figure 8) [61]. Furthermore, In the case of an injectable hydrogel system, the injectability is originated from the

breakage-recovery process. Thus diverse fabrication mechanisms are needed to be introduced, e.g., shear-thinning ability, host-guest reaction, and reversible chemical and/or physical bond [62-65]. However, these strategies often displayed disadvantageous features, which require multiple chemical reactions and potential cytotoxicity [37, 66]. On the other hand, microparticle-based systems have been developed to be used as injectable biomaterials since it has inter particular space between the microparticles, which allows itself to have deformability and injectability [67]. However, these microparticulate systems also need to utilize emulsification techniques, which use the organic phase and require additional removal procedures [68, 69].

To solve this problem, a microcarrier has been developed that increases the loading efficiency of cells and provides a high diffusion rate with a large surface area. However, cell death occurs due to pressure, friction, and etc. during the injection process, which leads to significantly reduced transfer efficiency because the cells adhere only to its surface. Thus the microcarrier has to provide sufficient internal porous structure to support cell proliferation after the cells are attached and be able to protect the cells from the external environment[70].

Cryogel is a three-dimensional polymer scaffold with a large porous structure and can be manufactured in various forms through suitable manufacturing processes [71] . In particular, a sphere-shaped microcarrier can be fabricated by a conventional emulsion method. Furthermore, recently, microfluidic devices allow producing a large number of microspheres with finely controlled sizes and shapes [72].

In this study, we proposed an injectable cryogel microspheres (ICM) system for cell delivery (scheme 2). The cryogel was fabricated using the naturally-derived biomaterials, gelatin and hyaluronic acid, with introducing methacrylic moiety. By coupling the microfluidic devices with cryo-emulsification technique, the size of ICM was determined. We estimated the cell-protective ability of ICM against injection pressures and in vivo environment. It highlights that the ICM system would be utilized to stem cell therapy or tissue engineering application

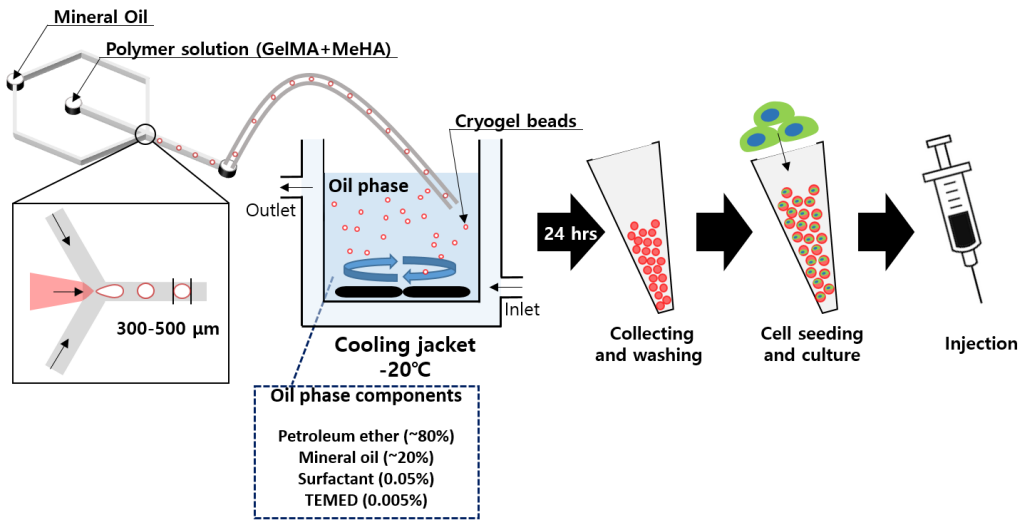

Scheme 2. Schematic of cryogel microsphere preparation via microfluidic channel and emulsification.

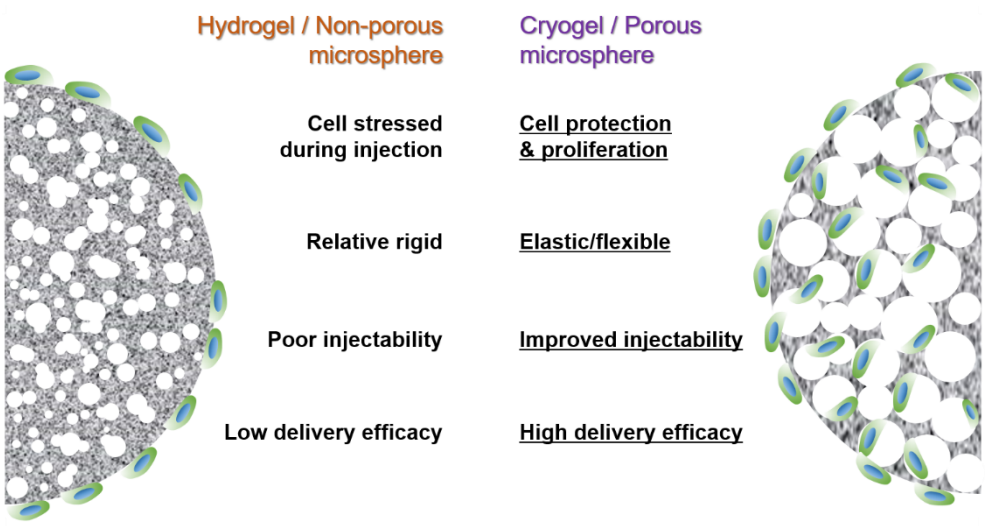

Figure 8. Comparative table between hydrogel and cryogel microsphere

2.2 Experimental section

2.2.1 Synthesis of methacrylated biopolymers

Gelatin methacrylate (GelMA) was performed as previously recommend [73]. The gelatin from porcine skin (type A, Sigma-Aldrich) was dissolved with 10 w/v% in phosphate-buffered saline (PBS; Gibco) at 60℃. Methacrylic anhydride (MA, Sigma-Aldrich) was added to gelatin solution for the final concentration at 8 v/v %. After 3 hours reaction, PBS was added five times of the solution to stop the reaction and dialyzed against D.W for 7 days at 50℃ followed by lyophilization and storage at −20℃. The methacrylation was confirmed by ^{1}H NMR by dissolving gelatin and GelMA in D_2O.

Methacrylated Hyaluronic acid (MeHA) was also synthesized as previously described [74]. Briefly, HA (MW 64000; Life Core Technologies) was dissolved in PBS at 1 w/v% and stirred. Then glycidyl methacrylate (GMA; Sigma-Aldrich) was added with 2 v/v% and toughly stirred at room temperature for 8days. The solution was dialyzed against D.W through 1000 M.W membrane for 2days followed by lyophilization. The methacrylation was also confirmed by ^{1}H NMR by dissolving HA and MeHA in D_2O.

2.2.2 Fabrication of cryogel

To optimize the condition of cryogel, we fabricated bulky cryogel for characterization. We dissolved MeHA and GelMA at 2 w/v%, 4 w/v% in D.I water and mixed with various ratio. The final concentration of GelMA/MeHA was 2/1, 2/0.5, 1/1 and 1/0.5. APS and TEMED were added to the solution at 0.4 w/v % and 0.1 v/v %, respectively The polymerization was processed at −20℃ for 24 h.

2.2.3 Swelling ratio and rheological property of cryogel

The swelling ratio was characterized by measuring both the dry and wet weight of the cryogel. The wet weight was measured after soaking the cryogel in DI water until it reached the swollen equilibrium state. The swelling ratio was calculated as the following equation;

$$\text{Swelling ratio } (Q) = W_s/W_d$$

, where W_s and W_d represent swollen and dry weight, respectively.

The mechanical property of the cryogel was estimated using a rheometer (MCR 302, Anton−Paar, Austria) depends on the GelMA/MeHA concentration. The cryogels were prepared in a cylindrical shape with a diameter of 8 mm. The frequency sweep test

was carried out with increasing the oscillator frequency from 0.1 to 10 Hz at a constant strain of 1 %. The shear storage modulus (G') was recorded.

2.2.4 Preparation of cryogel microspheres

The cryogel microspheres was prepared using the microfluidic devices coupled with cryo-emulsification. The microfluidic channel was purchatsed from MicroFIT Co.Ltd.(South Korea), which represent cross-shaped junction with a 300μm channel thickneses as previously described [75, 76]. MeHA and GelMA dissolved in DI water at 0.5 w/v% and 1 w/v% respectively, with APS was injected into the main channel, simultaneously the mineral oil was injected into the side channel . The polymeric microsphere was obtained at the junction of both channels, followed by dropped into the emulsion jacket.

The jacket was pre-cooled down to -20℃ in advance using Refrigerated circulator (AD07R-40-A13D, Polyscience) filled with the 80 mL of petroleum ether and 20 mL of mineral oil. TEMED and surfactant were also added at 0.5 v/v % and 0.1 % into the solution in the jacket.

After 24hours for stirring, the cryogel microspheres were collected

and washed with petroleum ether, ethanol and DI water sequentially (or consecutively) each for 1 day, followed by lyophilization.

2.2.5 Cell proliferation and viability

The *in vitro* cell proliferation was monitored as the way of cell viability test using Human dermal fibroblasts (HDFs). $5x10^4$ cells per well were seeded on a 24-well plate and incubated with cryogel microspheres in DMEM with 10% FBS and 1% PS.

After 3 days and 7 days, Live/Dead assay kit (Invitrogen)was used to assess the proliferation of HDFs and the fluorescent images were obtained using a fluorescence microscope (AMF4300, EVOS, Life Technology). The cell viability was calculated from the number of live cells per total. We also confirmed that the cells were almost alive after injection via Live/Dead assay kit.

2.2.6 Cell infiltration

We coated 24 plate well with 1 w/v% agarose gel to prevent cell adhesion. We sterilized cryogels under UV for 24 hours and put cryogel microspheres on the coated 24 well plate as one layer. As mentioned above, $5x10^4$cells per well were seeded on a cryogels and

incubated in DMEM with 10% FBS and 1% PS. After 3 days, to identify cell infiltration into cryogel microspheres, we used Confocal laser scanning microscope (LSM710 ,Carl Zeiss, Germany).

2.3 Results & Discussion

2.3.1 Synthesis of methacrylated biopolymers

We synthesized both GelMA and MeHA by methacrylation process and conducted the ^{1}H−NMR analysis. The ^{1}H−NMR spectra of GelMA represented the peaks from 5.2 to 6 ppm corresponding to methylene and methacrylamide (Figure 8) [77]. At the same time, the ^{1}H−NMR spectra of MeHA showed the peaks at 5.8 and 6.3 ppm corresponding to the methacrylate group (Figure 8), which indicated that both the GelMA and MeHA were successfully synthesized.

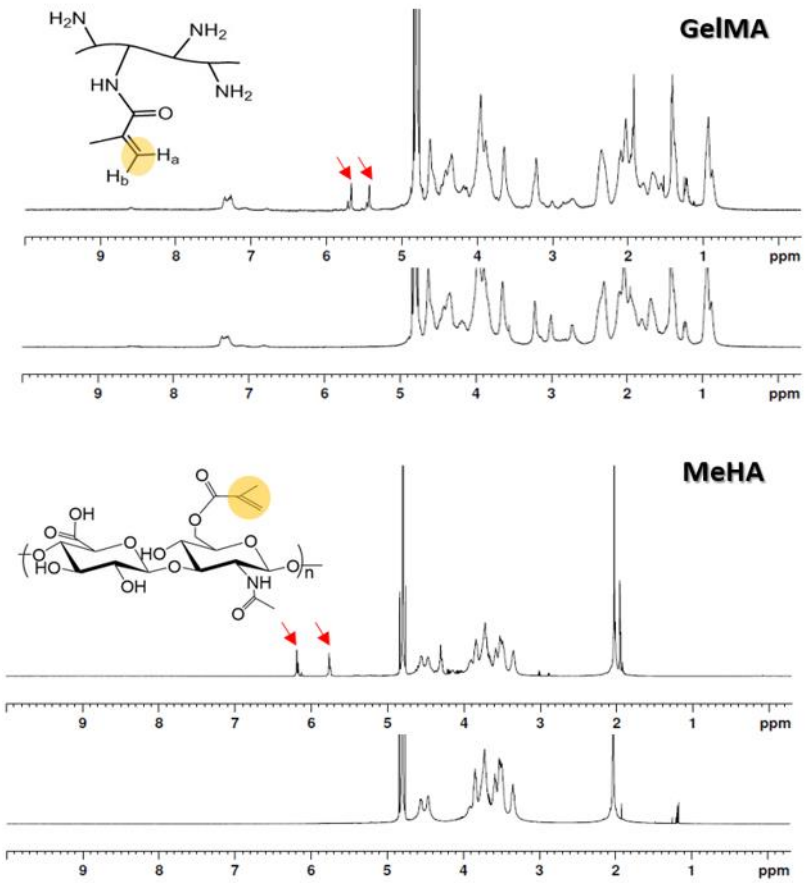

Figure 9. ^{1}H−NMR analysis of the methacrylated biopolymers. ^{1}H−NMR spectra of (A)gelatin methacrylate (GelMA) and (B) methacrylated HA (MeHA). The peaks corresponding to the methacrylate group were confirmed, which indicated that both GelMA and MeHA were successfully synthesized.

2.3.2 Characterization of cryogel

The cryogels could imbibe the water ,however, the volumetric swelling ratio of the cryogels increased with increasing the MeHA contents due to the abundant hydrophilic and negative charge moieties. Also, as gelatin concentration increases, the cryogel becomes opaque.

The Q value of GelMA/MeHA cryogel with a concentration ratio of 2/1 and 1/1 w/v% represented 31.32 ± 3.40 and 36.31 ± 6.36, respectively (Figure 9). While at the same time, the cryogels of 2/0.5 and 1/0.5 w/v% were 26.63 ± 2.75 and 28.35 ± 4.15, respectively. Although the cryogels in all groups were significantly swollen, the Q was much higher in MeHA-rich cryogels than that of MeHA-deficient cryogels. It suggests that the hydrophilic moiety of MeHA was contributed to interacting with much more water molecules, which would result in a high swelling ratio.

Next, we investigated the mechanical property of cryogels depending on the polymer contents using a rheometer (Figure 10). The cryogel with GelMA-rich groups showed a much higher mechanical property. In particular, the 2/0.5 cryogel had a robust mechanical behavior than 2/1 cryogel despite the overall higher polymeric concentration. It might be attributed that the more MeHA

content was in the cryogel, the lower the network density appeared, which caused a diminished mechanical property.

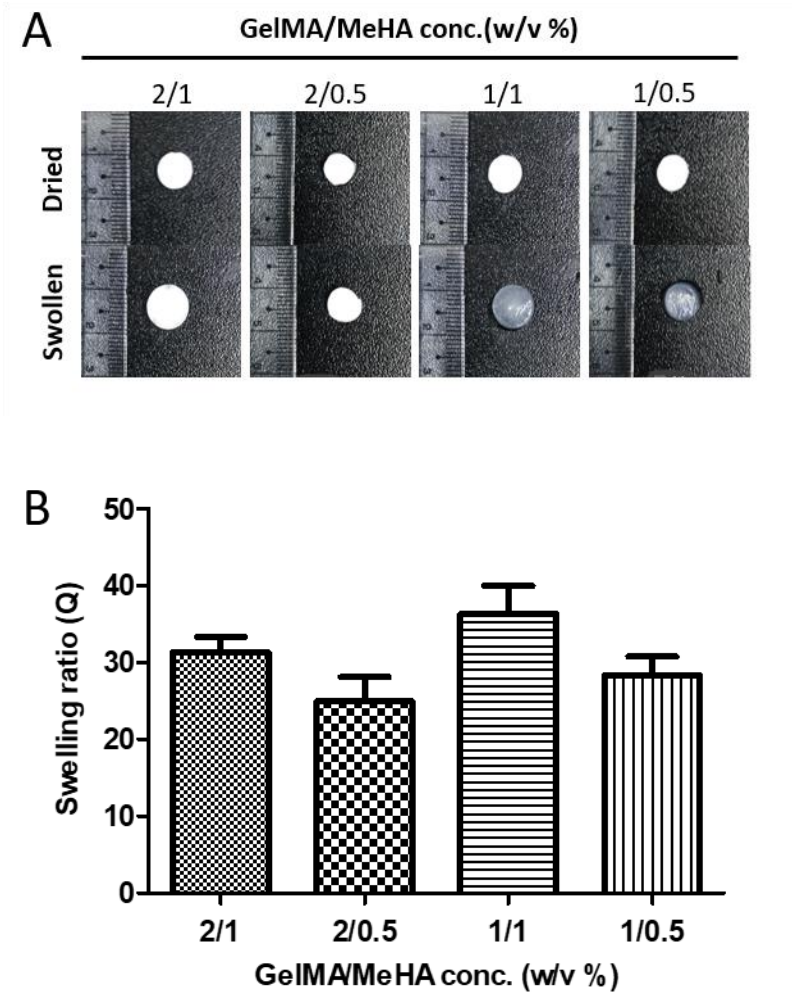

Figure 10. Fabrication of cryogel and its swelling ratio.

(A) photographs of cryogel in both dried and swollen states,

(B) which showed the higher volumetric swelling was obtained with increasing the MeHA concentration.

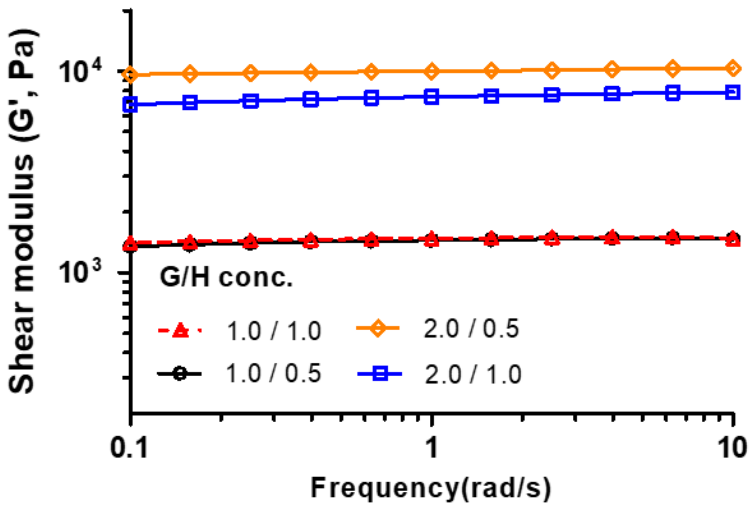

Figure 11. Rheological property of cryogel. Storage modulus(G') of cryogel dependent on concentration of GelMA/MeHA.

2.3.3 Preparation of cryogel microsphere

We obtained cryogel microspheres via microfluidic channel and emulsification. Size of the microsphere was determined by the microfluidic channel internal diameter (figure 11A). The inner width of the microfluidic channel was about 300 μm and the microspheres in wet state were about 300−500 μm (figure 11B). We also visualized the homogeneously mingled state using RITC conjugated GelMA through a microscope (figure 11C). Given that the animal cell size is about 20 μm, the cryogel microspheres were sufficient to provide an environment for cell delivery. Furthermore, the pore size of cryogel was about 42.18μm enough to make cells infiltrate into cryogel (figure 11D).

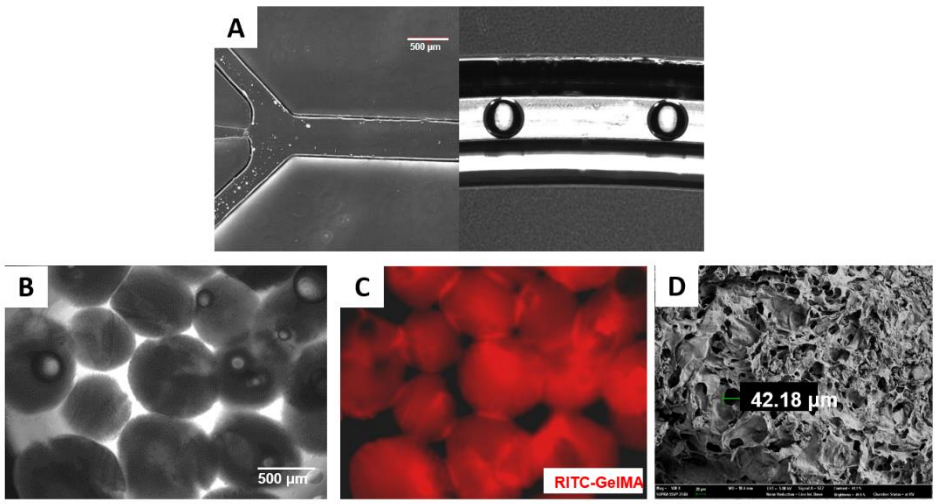

Figure 12. Morphology of cryogel microsphere. (A) microfluidic channel and microspheres are passing through it. (B) microscope transmittance image of cryogel microspheres. (C) RITC conjugated GelMA cryogel microspheres. (D) SEM image of microsphere and its pore size.

2.3.4 In vitro, cell viability and protection.

Through the Live/Dead analysis, we confirmed that GelMA/MeHA cryogel was biocompatible had litte cytotoxicity. There is no difference between day3 and day7 Live/Dead images, which means that cells were alive within cryogel microspheres and did not provide any negative effects on the cells. We could also see the elongation of HDFs for growth on day 7 (figure 13).

Furtheremore, we confirmed that cells were protected in cryogel after injection through 21G syringe needle (figure 13). It suggests that cells do not adhere only to its surface and could infiltrate into sufficient internal space in cryogel through macropores. Thus, cell death almost does not occur during injection process. It results from that cryogel makes loading efficiency of cells increase and provide a high diffusion rate with large surface area.

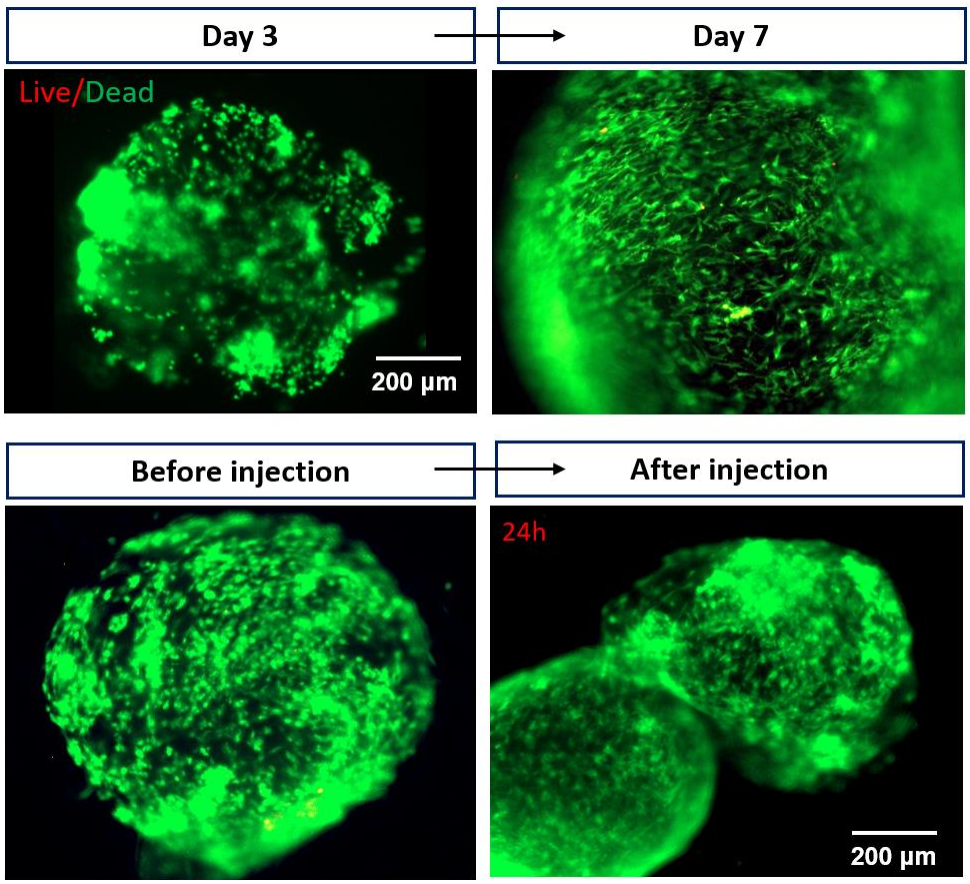

Figure 13. *In vitro*, Live/Dead images for verifying cell viability and protection.

2.4 Conclusion

In this study, we developed injectable cryogel microspheres system for improving the cell delivery efficacy. Through varying the MeHA/GelMA ratio, we optimized the cryogel with characterizing the swelling behavior and mechanical property. Then, we could fabricate cryogel microspheres with narrow size distribution by coupling the microfluidic channel with cryo-emulsification technique. Furthermore, we verified the in vitro cell viability and cell protection ability of the cryogel microspheres, which was attributed to that the cells could infiltrate into the cryogel microspheres due to its macroporous structure. In short, we have developed a cryogel microsphere scaffolds for delivering the cells with high loading efficiency. This approach would be applied to cell-based therapeutic applications.

References

[1] M. Razavi, Y. Qiao, A.S. Thakor, Three-dimensional cryogels for biomedical applications, J Biomed Mater Res A 107(12) (2019) 2736-2755.
[2] Y. Saylan, A. Denizli, Supermacroporous Composite Cryogels in Biomedical Applications, Gels 5(2) (2019).
[3] L.J. Eggermont, Z.J. Rogers, T. Colombani, A. Memic, S.A. Bencherif, Injectable Cryogels for Biomedical Applications, Trends Biotechnol (2019).
[4] M. Spector, T.C. Lim, Injectable biomaterials: a perspective on the next wave of injectable therapeutics, Biomed Mater 11(1) (2016) 014110.
[5] H. Ercan, S. Durkut, A. Koc-Demir, A.E. Elcin, Y.M. Elcin, Clinical Applications of Injectable Biomaterials, Adv Exp Med Biol 1077 (2018) 163-182.
[6] L.J. Eggermont, Z.J. Rogers, T. Colombani, A. Memic, S.A. Bencherif, Injectable Cryogels for Biomedical Applications, Trends Biotechnol 38(4) (2020) 418-431.
[7] M. Rezaeeyazdi, T. Colombani, A. Memic, S.A. Bencherif, Injectable Hyaluronic Acid-co-Gelatin Cryogels for Tissue-Engineering Applications, Materials 11(8) (2018).
[8] S.A. Bencherif, R. Warren Sands, O.A. Ali, W.A. Li, S.A. Lewin, T.M. Braschler, T.Y. Shih, C.S. Verbeke, D. Bhatta, G. Dranoff, D.J. Mooney, Injectable cryogel-based whole-cell cancer vaccines, Nat Commun 6 (2015) 7556.
[9] S.T. Koshy, T.C. Ferrante, S.A. Lewin, D.J. Mooney, Injectable, porous, and cell-responsive gelatin cryogels, Biomaterials 35(8) (2014) 2477-87.
[10] S.T. Koshy, D.K.Y. Zhang, J.M. Grolman, A.G. Stafford, D.J. Mooney, Injectable nanocomposite cryogels for versatile protein drug delivery, Acta Biomater 65 (2018) 36-43.
[11] W.J. King, P.H. Krebsbach, Grwoth factor delivery: How surface interactions modulate release in vitro and in vivo, Adv. Drug Deliv. Rev. 64(12) (2012) 1239-1256.
[12] A. Zieris, R. Dockhorn, A. Rohrich, R. Zimmermann, M. Muller, P.B. Welzel, M.V. Tsurkan, J.U. Sommer, U. Freudenberg, C. Werner, Biohybrid Networks of Selectively Desulfated Glycosaminoglycans for Tunable Growth Factor Delivery, Biomacromolecules 15(12) (2014) 4439-4446.
[13] D. Hachim, T.E. Whittaker, H. Kim, M.M. Stevens, Glycosaminoglycan-based biomaterials for growth factor and cytokine delivery: Making the right choices, J Control Release 313 (2019) 131-147.
[14] I. Kim, S.S. Lee, S. Bae, H. Lee, N.S. Hwang, Heparin Functionalized Injectable Cryogel with Rapid Shape-Recovery Property for Neovascularization, Biomacromolecules 19(6) (2018) 2257-2269.
[15] V.E. Santo, M.E. Gomes, J.F. Mano, R.L. Reis, Chitosan-chondroitin sulphate nanoparticles for controlled delivery of platelet lysates in bone regenerative medicine, J Tissue Eng Regen M 6 (2012) s47-s59.
[16] S. Bang, U.W. Jung, I. Noh, Synthesis and Biocompatibility

Characterizations of in Situ Chondroitin Sulfate-Gelatin Hydrogel for Tissue Engineering, Tissue Eng Regen Med 15(1) (2018) 25-35.
[17] Q. Tan, H. Tang, J. Hu, Y. Hu, X. Zhou, Y. Tao, Z. Wu, Controlled release of chitosan/heparin nanoparticle-delivered VEGF enhances regeneration of decellularized tissue-engineered scaffolds, Int J Nanomedicine 6 (2011) 929-42.
[18] Y.J. Park, Y.M. Lee, J.Y. Lee, Y.J. Seol, C.P. Chung, S.J. Lee, Controlled release of platelet-derived growth factor-BB from chondroitin sulfate-chitosan sponge for guided bone regeneration, J Control Release 67(2-3) (2000) 385-94.
[19] T. Miller, M.C. Goude, T.C. McDevitt, J.S. Temenoff, Molecular engineering of glycosaminoglycan chemistry for biomolecule delivery, Acta Biomater 10(4) (2014) 1705-19.
[20] D. Hachim, T.E. Whittaker, H. Kim, M.M. Stevens, Glycosaminoglycan-based biomaterials for growth factor and cytokine delivery: Making the right choices, Journal of Controlled Release 313 (2019) 131-147.
[21] L.M. Yu, K. Kazazian, M.S. Shoichet, Peptide surface modification of methacrylamide chitosan for neural tissue engineering applications, J Biomed Mater Res A 82(1) (2007) 243-55.
[22] H.D. Kim, E.A. Lee, Y.H. An, S.L. Kim, S.S. Lee, S.J. Yu, H.L. Jang, K.T. Nam, S.G. Im, N.S. Hwang, Chondroitin Sulfate-Based Biomineralizing Surface Hydrogels for Bone Tissue Engineering, Acs Appl Mater Inter 9(26) (2017) 21639-21650.
[23] R.B. Qaqish, M.M. Amiji, Synthesis of a fluorescent chitosan derivative and its application for the study of chitosan-mucin interactions, Carbohyd Polym 38(2) (1999) 99-107.
[24] H. Skaat, O. Ziv-Polat, A. Shahar, S. Margel, Enhancement of the growth and differentiation of nasal olfactory mucosa cells by the conjugation of growth factors to functional nanoparticles, Bioconjug Chem 22(12) (2011) 2600-10.
[25] Y.H. Choi, S.H. Kim, I.S. Kim, K. Kim, S.K. Kwon, N.S. Hwang, Gelatin-based micro-hydrogel carrying genetically engineered human endothelial cells for neovascularization, Acta Biomater 95 (2019) 285-296.
[26] H. Niiyama, N.F. Huang, M.D. Rollins, J.P. Cooke, Murine model of hindlimb ischemia, J Vis Exp (23) (2009).
[27] M.J. Webber, J. Tongers, C.J. Newcomb, K.-T. Marquardt, J. Bauersachs, D.W. Losordo, S.I. Stupp, Supramolecular nanostructures that mimic VEGF as a strategy for ischemic tissue repair, Proc Natl Acad Sci U S A 108(33) (2011) 13438-13443.
[28] L. Zhu, K.M. Bratlie, pH sensitive methacrylated chitosan hydrogels with tunable physical and chemical properties, Biochemical Engineering Journal 132 (2018) 38-46.
[29] L.J. Eggermont, Z.J. Rogers, T. Colombani, A. Memic, S.A. Bencherif, Injectable Cryogels for Biomedical Applications, Trends Biotechnol 38(4) (2020) 418-431.
[30] S.A. Bencherif, R.W. Sands, D. Bhatta, P. Arany, C.S. Verbeke, D.A. Edwards, D.J. Mooney, Injectable preformed scaffolds with shape-memory

properties, P Natl Acad Sci USA 109(48) (2012) 19590-19595.
[31] M.E. Han, S.H. Kim, H.D. Kim, H.G. Yim, S.A. Bencherif, T.I. Kim, N.S. Hwang, Extracellular matrix-based cryogels for cartilage tissue engineering, Int J Biol Macromol 93(Pt B) (2016) 1410-1419.
[32] Y. Alinejad, A. Adoungotchodo, E. Hui, F. Zehtabi, S. Lerouge, An injectable chitosan/chondroitin sulfate hydrogel with tunable mechanical properties for cell therapy/tissue engineering, Int J Biol Macromol 113 (2018) 132-141.
[33] M.N. Rodrigues, M.B. Oliveira, R.R. Costa, J.F. Mano, Chitosan/Chondroitin Sulfate Membranes Produced by Polyelectrolyte Complexation for Cartilage Engineering, Biomacromolecules 17(6) (2016) 2178-88.
[34] A. Denuziere, D. Ferrier, O. Damour, A. Domard, Chitosan-chondroitin sulfate and chitosan-hyaluronate polyelectrolyte complexes: biological properties, Biomaterials 19(14) (1998) 1275-85.
[35] S. Sharma, K.L. Swetha, A. Roy, Chitosan-Chondroitin sulfate based polyelectrolyte complex for effective management of chronic wounds, Int J Biol Macromol 132 (2019) 97-108.
[36] J.H. Lee, Injectable hydrogels delivering therapeutic agents for disease treatment and tissue engineering, Biomater Res 22 (2018) 27.
[37] F. Munarin, P. Petrini, S. Bozzini, M.C. Tanzi, New perspectives in cell delivery systems for tissue regeneration: natural-derived injectable hydrogels, J Appl Biomater Funct Mater 10(2) (2012) 67-81.
[38] H. Naderi-Meshkin, K. Andreas, M.M. Matin, M. Sittinger, H.R. Bidkhori, N. Ahmadiankia, A.R. Bahrami, J. Ringe, Chitosan-based injectable hydrogel as a promising in situ forming scaffold for cartilage tissue engineering, Cell Biol Int 38(1) (2014) 72-84.
[39] J.D. Kretlow, S. Young, L. Klouda, M. Wong, A.G. Mikos, Injectable biomaterials for regenerating complex craniofacial tissues, Adv Mater 21(32-33) (2009) 3368-93.
[40] A. Fakhari, C. Berkland, Applications and emerging trends of hyaluronic acid in tissue engineering, as a dermal filler and in osteoarthritis treatment, Acta Biomater 9(7) (2013) 7081-92.
[41] B.J. Kang, H. Kim, S.K. Lee, J. Kim, Y. Shen, S. Jung, K.S. Kang, S.G. Im, S.Y. Lee, M. Choi, N.S. Hwang, J.Y. Cho, Umbilical-cord-blood-derived mesenchymal stem cells seeded onto fibronectin-immobilized polycaprolactone nanofiber improve cardiac function, Acta Biomater 10(7) (2014) 3007-3017.
[42] Y.H. Choi, S.C. Heo, Y.W. Kwon, H.D. Kim, S.H. Kim, I.H. Jang, J.H. Kim, N.S. Hwang, Injectable PLGA microspheres encapsulating WKYMVM peptide for neovascularization, Acta Biomater 25 (2015) 76-85.
[43] L. Deveza, J. Choi, F. Yang, Therapeutic angiogenesis for treating cardiovascular diseases, Theranostics 2(8) (2012) 801-14.
[44] N. Ferrara, H.P. Gerber, J. LeCouter, The biology of VEGF and its receptors, Nat Med 9(6) (2003) 669-76.
[45] X. Hu, K.G. Neoh, Z. Shi, E.T. Kang, C. Poh, W. Wang, An in vitro assessment of titanium functionalized with polysaccharides conjugated with

vascular endothelial growth factor for enhanced osseointegration and inhibition of bacterial adhesion, Biomaterials 31(34) (2010) 8854-63.
[46] P.O. Rujitanaroj, R. Aid-Launais, S.Y. Chew, C. Le Visage, Polysaccharide electrospun fibers with sulfated poly(fucose) promote endothelial cell migration and VEGF-mediated angiogenesis, Biomater Sci-Uk 2(6) (2014) 843-852.
[47] J.J. Lim, T.M. Hammoudi, A.M. Bratt-Leal, S.K. Hamilton, K.L. Kepple, N.C. Bloodworth, T.C. McDevitt, J.S. Temenoff, Development of nano- and microscale chondroitin sulfate particles for controlled growth factor delivery, Acta Biomater 7(3) (2011) 986-95.
[48] M. Tanihara, Y. Suzuki, E. Yamamoto, A. Noguchi, Y. Mizushima, Sustained release of basic fibroblast growth factor and angiogenesis in a novel covalently crosslinked gel of heparin and alginate, J Biomed Mater Res 56(2) (2001) 216-21.
[49] A. Bozkir, O.M. Saka, Chitosan nanoparticles for plasmid DNA delivery: effect of chitosan molecular structure on formulation and release characteristics, Drug Deliv 11(2) (2004) 107-12.
[50] A. Bernkop-Schnurch, S. Dunnhaupt, Chitosan-based drug delivery systems, Eur J Pharm Biopharm 81(3) (2012) 463-9.
[51] H. Yang, C. Tang, C. Yin, Estrone-modified pH-sensitive glycol chitosan nanoparticles for drug delivery in breast cancer, Acta Biomater 73 (2018) 400-411.
[52] L. Qi, Z. Xu, X. Jiang, C. Hu, X. Zou, Preparation and antibacterial activity of chitosan nanoparticles, Carbohydr Res 339(16) (2004) 2693-700.
[53] N. Lohmann, L. Schirmer, P. Atallah, E. Wandel, R.A. Ferrer, C. Werner, J.C. Simon, S. Franz, U. Freudenberg, Glycosaminoglycan-based hydrogels capture inflammatory chemokines and rescue defective wound healing in mice, Sci Transl Med 9(386) (2017).
[54] N. Suffee, C. Le Visage, H. Hlawaty, R. Aid-Launais, V. Vanneaux, J. Larghero, O. Haddad, O. Oudar, N. Charnaux, A. Sutton, Pro-angiogenic effect of RANTES-loaded polysaccharide-based microparticles for a mouse ischemia therapy, Sci Rep 7(1) (2017) 13294.
[55] S. Hou, X.F. Niu, L.H. Li, J. Zhou, Z.Y. Qian, D.Y. Yao, F.H. Yang, P.X. Ma, Y.B. Fan, Simultaneous nano- and microscale structural control of injectable hydrogels via the assembly of nanofibrous protein microparticles for tissue regeneration, Biomaterials 223 (2019).
[56] R. Lev, D. Seliktar, Hydrogel biomaterials and their therapeutic potential for muscle injuries and muscular dystrophies, J R Soc Interface 15(138) (2018).
[57] T.W. Gilbert, D.B. Stolz, F. Biancaniello, A. Simmons-Byrd, S.F. Badylak, Production and characterization of ECM powder: implications for tissue engineering applications, Biomaterials 26(12) (2005) 1431-5.
[58] S. Mazzitelli, G. Luca, F. Mancuso, M. Calvitti, R. Calafiore, C. Nastruzzi, S. Johnson, S.F. Badylak, Production and characterization of engineered alginate-based microparticles containing ECM powder for cell/tissue engineering applications, Acta Biomater 7(3) (2011) 1050-62.
[59] X.L. Wang, N. Rivera-Bolanos, B. Jiang, G.A. Ameer, Advanced

Functional Biomaterials for Stem Cell Delivery in Regenerative Engineering and Medicine, Adv Funct Mater 29(23) (2019).
[60] K. Liang, K.H. Bae, M. Kurisawa, Recent advances in the design of injectable hydrogels for stem cell-based therapy, J Mater Chem B 7(24) (2019) 3775-3791.
[61] M. Liu, X. Zeng, C. Ma, H. Yi, Z. Ali, X. Mou, S. Li, Y. Deng, N. He, Injectable hydrogels for cartilage and bone tissue engineering, Bone Res 5 (2017) 17014.
[62] V. Pertici, C. Pin-Barre, C. Rivera, C. Pellegrino, J. Laurin, D. Gigmes, T. Trimaille, Degradable and Injectable Hydrogel for Drug Delivery in Soft Tissues, Biomacromolecules 20(1) (2019) 149-163.
[63] S. Hou, X. Wang, S. Park, X. Jin, P.X. Ma, Rapid Self-Integrating, Injectable Hydrogel for Tissue Complex Regeneration, Adv Healthc Mater 4(10) (2015) 1491-5, 1423.
[64] H.D. Lu, M.B. Charati, I.L. Kim, J.A. Burdick, Injectable shear-thinning hydrogels engineered with a self-assembling Dock-and-Lock mechanism, Biomaterials 33(7) (2012) 2145-53.
[65] C. Yan, A. Altunbas, T. Yucel, R.P. Nagarkar, J.P. Schneider, D.J. Pochan, Injectable solid hydrogel: mechanism of shear-thinning and immediate recovery of injectable beta-hairpin peptide hydrogels, Soft Matter 6(20) (2010) 5143-5156.
[66] K. Liang, K.H. Bae, M. Kurisawa, Recent advances in the design of injectable hydrogels for stem cell-based therapy, J. Mater. Chem. B 7(24) (2019) 3775-3791.
[67] W. Jiang, R.K. Gupta, M.C. Deshpande, S.P. Schwendeman, Biodegradable poly(lactic-co-glycolic acid) microparticles for injectable delivery of vaccine antigens, Adv Drug Deliv Rev 57(3) (2005) 391-410.
[68] F.Y. Han, A. Whittaker, S.M. Howdle, A. Naylor, A. Shabir-Ahmed, M.T. Smith, Sustained-Release Hydromorphone Microparticles Produced by Supercritical Fluid Polymer Encapsulation, J Pharm Sci 108(2) (2019) 811-814.
[69] J. Guan, N. Ferrell, L. James Lee, D.J. Hansford, Fabrication of polymeric microparticles for drug delivery by soft lithography, Biomaterials 27(21) (2006) 4034-41.
[70] D.X. Wei, J.W. Dao, G.Q. Chen, A Micro-Ark for Cells: Highly Open Porous Polyhydroxyalkanoate Microspheres as Injectable Scaffolds for Tissue Regeneration, Adv Mater 30(31) (2018) e1802273.
[71] B. Newland, P.B. Welzel, H. Newland, C. Renneberg, P. Kolar, M. Tsurkan, A. Rosser, U. Freudenberg, C. Werner, Tackling Cell Transplantation Anoikis: An Injectable, Shape Memory Cryogel Microcarrier Platform Material for Stem Cell and Neuronal Cell Growth, Small 11(38) (2015) 5047-53.
[72] T.T. Guan, Y.W. Gao, M.M. Pan, Y.W. Wu, S.H. Zhang, L.H. Xu, L.Y. Zhu, J.X. Yun, Slug flow hydrodynamics of immiscible fluids within a rectangular microchannel towards size-controllable fabrication of dextran-based cryogel beads, Chem Eng J 369 (2019) 116-123.
[73] Y.H. An, S.J. Yu, I.S. Kim, S.H. Kim, J.M. Moon, S.L. Kim, Y.H. Choi, J.S.

Choi, S.G. Im, K.E. Lee, N.S. Hwang, Hydrogel Functionalized Janus Membrane for Skin Regeneration, Adv Healthc Mater 6(5) (2017).
[74] M.E. Han, B.J. Kang, S.H. Kim, H.D. Kim, N.S. Hwang, Gelatin-based extracellular matrix cryogels for cartilage tissue engineering, J Ind Eng Chem 45 (2017) 421-429.
[75] J. Yun, C. Tu, D.Q. Lin, L. Xu, Y. Guo, S. Shen, S. Zhang, K. Yao, Y.X. Guan, S.J. Yao, Microchannel liquid-flow focusing and cryo-polymerization preparation of supermacroporous cryogel beads for bioseparation, J Chromatogr A 1247 (2012) 81-8.
[76] (!!! INVALID CITATION !!! [69]).
[77] S. Krishnamoorthy, B. Noorani, C. Xu, Effects of Encapsulated Cells on the Physical-Mechanical Properties and Microstructure of Gelatin Methacrylate Hydrogels, Int J Mol Sci 20(20) (2019).

국문초록(요약)

치료제 전달을 위한 주입식 마이크로 크라이오겔 시스템 개발

크라이오겔은 큰 기공구조를 가지고 있으며, 형상기억능과 주입 가능하다는 특징이 있다. 또한, 세포나 성장인자들이 크라이오겔 내부에 담지되어 서방출 양상을 띄기도 한다. 이러한 특징들 덕분에, 크라이오겔은 조직공학적으로 널리 사용되고 있다.

그러나, 부피가 큰 크라이오겔은 작은 주사바늘구멍을 통과하기 힘들고, 불규칙적 모양의 병변 부위를 완전히 채울 수 없다. 따라서 위 논문에서 우리는 세포나 치료제 전달을 할 수 있는 주사가능 크라이오겔 시스템을 개발하였다. 이것은 부드럽게 주입되고 사출 성형능과 void-filling 특성을 띈다.

첫번째 챕터에서는, 주입식 크라이오겔 마이크로입자(CMP)를 pulverizing을 통해 손쉽게 제작하였다. CMP를 제작하기 위해 우리는 메타크릴레이트화 키토산과 메타크릴레이트와 황산콘드로이틴을 사용하여 영하 20도씨 조건에서 가교시켰다. 또한 혈관생성인자를 CMP 에 담지하여 서방출양상을 띄었다. 마지막으로, 혈관생성인자가 담지된 크라이오겔을 하지허혈 마우스모델에 근육주사하여 신생혈관이 촉진되고, 괴사를 억제하여 조직재생이 되는 것 역시 확인하였다.

두번째 챕터에서는, 주입식 크라이오겔 마이크로스피어를 미세유체칩과 에멀젼기법을 통해 제작하였다. 메타크릴레이트화된 젤라틴과 메타크릴레이트화된 히알루론산을 이용하여 마이크로스피어를 제작하였고, 이는 보다 균일한 상태의 미세입자형태를 보였다. 뿐만 아니라, 세포가 크라이오겔 마이크로스피어 내부로 침투하고 외부의 충격으로부터 보호되어 크라이오겔이 세포를 전달하기 적합한 환경임을 확인하였다.

주요어; 주입식 크라이오겔, 서방출, 마이크로입자, 신생혈관생성, 마이크로스피어, 세포전달